

Modeling and Computational Analysis of Turbulent Free convection in Tall Enclosure Filled with Nano-Fluid

Asst. Prof. Dr. Karima E. Amori
 Department of Mechanical Engineering
 University of Baghdad
 College of Engineering
 E-mail: drkarimaa@yahoo.com

Qasim Kadhim Huneheh
 Department of Mechanical Engineering
 University of Baghdad
 College of Engineering
 E-mail: alqassim73@yahoo.com

Abstract- In this work, the turbulent buoyancy driven fluid flow and heat transfer in a differentially heated tall rectangular enclosure filled with nanofluid is quantified numerically. The two dimensional governing differential equations (continuity, momentum, energy and low Reynolds number LRN $k-\omega$ turbulence equations) are discretized using the finite volume method. SIMPLE algorithm is employed to obtain stabilized solution for high Rayleigh numbers. Two types of nanofluids namely, Al₂O₃-water and Cu-water, were considered. The effect of Rayleigh number (10¹⁰ to 10¹²), diameter of nanoparticles in the range 25-100 nm, nanoparticle volume fraction in range 0-0.08 and the aspect ratio (30, 40 and 50) on fluid flow and heat transfer are investigated. The present results are compared with previously published work and a qualitative agreement with good validation is obtained. Results show that addition of nanoparticles makes the liquid be more viscous which decreases the vertical velocity component and also decreases the temperature gradient near the walls. Also an announced heat transfer enhancement is obtained with nanoparticle volume fraction reaching a maximum point called optimal volume loading, at which the maximum convective heat transfer is obtained, and then it decreased with further increase of volume fraction.

Keywords: Natural convection; turbulent; tall enclosure; finite volume method; nanofluid.

1. Introduction

Buoyancy-induced heat transfer in enclosure differentially heated at sides is of great practical importance in different engineering applications, such as the cooling of electronic assemblies and the collection of solar energy. Enhancement of heat transfer in such systems is essential from industrial and energy saving perspectives. However, conventional heat transfer fluids such as water, oil and ethylene glycol have an inherently poor thermal performance due to their low thermal conductivities.

Fluids with dispersed nanoparticles in them are called nanofluids and their heat transfer performance is superior to suspensions of millimeter or micrometer particles in fluid. Their potential benefits are large relative surface area, higher heat conduction, excellent stability and minimal clogging. Hence, nanofluids can be considered as the next generation of heat transfer fluids, **Fotukian and Esfahany [1]**.

For forced convection heat transfer applications, several studies showed that the addition of nanoparticles into a base liquid can bring to an enhancement in heat transfer, **Fotukian and Esfahany [1]**, **Rostamani et al. [2]** and **Özerinç et al [3]**. However, for natural convection heat transfer enhancement using nanofluids is still limited especially in turbulent regime. Essentially, most of the

numerical studies in natural convection using nanofluids in literature focused on laminar flow. **Khanafer et al. [4]** considered the buoyancy-driven heat transfer in a two-dimensional enclosure filled with nanofluids for the Grashof numbers of 10³, 10⁴ and 10⁵ using the finite volume method. They concluded that the existence of the nanoparticles resulted in an increase in the rate of heat transfer for all the Grashof numbers considered. **Jou and Tzeng [5]** conducted a numerical study of the natural convection heat transfer in rectangular enclosures filled with a nanofluid using the finite difference method with the stream function-vorticity formulation. They investigated the effects of the Rayleigh number, the aspect ratio of the enclosure, and the volume fraction of the nanoparticles on the heat transfer inside the enclosures. Their results showed that the average heat transfer coefficient increased with increasing the volume fraction of the nanoparticles. **Oztop and Abu-Nada [6]** investigated the effects of the Rayleigh number, heater height, location of the heater, aspect ratio of the enclosure, and the volume fraction of the nanoparticles on the heat transfer inside the enclosures. They also found that the mean Nusselt number increased with increasing the volume fraction of the nanoparticles. Moreover, the location of the heater affected the flow and temperature fields inside the cavities.

Ogut E.B [7] examined various types of nanoparticles in natural convection nanofluids and showed that nanoparticles with a higher thermal conductivity (such as Ag and Cu) produce a greater enhancement in the rate of heat transfer. Moreover, **Kuang et al. [8]** showed that the heat transfer characteristics of the natural convection in Al₂O₃/water nanofluid can be enhanced as the mean nanoparticle diameter is decreased from 250 to 5 nm. The authors attributed these phenomena to the dominant effect of the Brownian motion caused by heat convection.

However, contradictory results have been observed in the experimental studies [9–11] that dispersion of nanoparticles in base fluid may result in marked reduction, instead of enhancement, of natural convection heat transfer in enclosures. **Putra et al. [9]** presented their experimental observations on natural convection of Al₂O₃ and CuO-water nanofluids inside a horizontal cylinder heated from one end and cooled from the other. Unlike the results of numerical studies, they found a systematic and definite deterioration of the natural convective heat transfer, which was dependent on the particle density, concentration, and the aspect ratio of the cylinder. The deterioration increased with particle concentration and was more significant for CuO nanofluids. For example, at Rayleigh number of 5×10⁷, 300% and 150% decrease in the Nusselt number was

found for ($\phi=4\%$) of CuO and Al₂O₃, respectively. **Wen and Ding [10]** also addressed the problem of natural convective heat transfer of TiO₂ (30–40 nm)/water nanofluids in a vessel which was composed of two horizontal aluminum discs of diameter 240 mm and thickness 10 mm separated by a 10 mm gap. They investigated both the transient and steady heat transfer coefficients for various concentrations of nanofluids. Similar to **Putra et al. [9]**, they also found that the natural convective heat transfer coefficient decreased as compared to that of pure water. Furthermore, such deterioration increased with nanoparticle concentrations. A completely different result was found experimentally by **Nnanna [11]**, who discovered the existence of an optimal particle loading for maximum heat transfer across the enclosure, which was explained as the consequence of an excessive increase in viscosity occurring above a certain nanoparticle concentration.

For turbulent natural convection, **Abu-Nada et al. [12]** investigated numerically the influence of volume fraction of nanoparticle for turbulent natural convection of Al₂O₃-water nanofluid. The governing equations and k- ω turbulence model are solved using a finite-volume method using FLUENT Package. Results have clearly indicated that the addition of nanoparticles has produced an enhancement on heat transfer with respect to that of the pure fluid. Experimentally, **Rui Ni et al. [13]**, performed heat transfer and flow dynamics measurements of the nanofluid (alumina particles in water) in turbulent natural convection in a Rayleigh-Bénard configuration. The measurements showed that the significant decrease of the nanofluid *Nu* comparing to that of water may be caused by the mass diffusion of nanoparticles. Furthermore, measurements of the flow velocity of the bulk nanofluid showed no significant difference from that of water for *Ra* either above or below *Ra_c*.

It seems clearly from previous studies that the heat transfer behavior of nanofluids is very complex and the application of nanofluids for heat transfer enhancement should not be decided only by their effective thermal conductivity.

Corcione [14] showed that the effective dynamic viscosity plays a role as crucial as that played by the effective thermal conductivity in determining the heat transfer performance of nanofluids in natural convection flows. Author developed two general empirical correlations, based on a wide variety of experimental data reported in the literature, for the evaluation of the nanofluid effective thermal conductivity and dynamic viscosity in natural heat transfer convection. These new correlations used to investigate the heat transfer features of buoyancy-driven nanofluids for different temperatures and solid volume fractions. The results showed that the heat transfer enhancement increases with increasing the nanoparticle volume fraction up to an optimal particle loading at which the amount of heat transferred across the enclosure has a peak and this optimal particle loading increase with increasing the aspect ratio of the differentially heated enclosure. The same results obtained by **Abouali and Ahmadi [15]** who showed the optimal particle loading is a function of the enclosure shape, type of nanofluids, Rayleigh number, the average temperature inside the enclosure and the nanoparticle diameter. Also, it must be noted that the recent studies confirmed the weakness of

Maxwell-Garnett model of *K_{eff}* and the use of the Brinkman viscosity model leads to the overestimation of the convective heat transfer in enclosures.

The aim of this work is to investigate numerically the turbulent natural convection in differentially heated tall enclosure filled with different types of nanofluids, since the studies on turbulent natural convection using nanofluids are limited. The LRN k- ω turbulence model is used to predict the kinetic energy and its specific dissipation rate. A parametric study is performed and the effects of pertinent parameters, such as the type of nanofluid, size and the volume fraction of the nanoparticles and the enclosure aspect ratio on the fluid flow and heat transfer inside the enclosure are investigated.

2. Mathematical Model

The geometry of the present problem is shown in **Fig. 1**. A vertical tall rectangular enclosure of height *H* and width *L* is investigated, where the left vertical wall is kept at constant high temperature of *T_H* while the right wall cooled to low temperature *T_C* and other sides kept adiabatic.

The nanofluid is handled as a single-phase fluid, which the same approach typically used in most studies performed on convective nanofluid. Thus, the equations that govern the flow and heat transfer valid for pure fluids can be directly extended to the nanoparticle suspension, provided that the thermophysical properties appearing in them are the nanofluid effective properties, **Corcione [14]**. It is assumed that the base fluid and the nanoparticles are in thermodynamic equilibrium and the density varies only in buoyant force, which has been incorporated only in the body force term by employing the Boussinesq approximation.

Therefore, assuming that the flow is two-dimensional, turbulent and incompressible, with negligible viscous dissipation, and that the nanofluid effective properties depend on temperature, the time-averaged governing equations, continuity, momentum and energy are written in tensor notation as:

$$\frac{\partial \bar{u}_i}{\partial x_i} = 0 \quad (1)$$

$$\rho_{nf} \frac{\partial \bar{u}_i}{\partial t} + \rho_{nf} \bar{u}_j \frac{\partial \bar{u}_i}{\partial x_j} = -\frac{\partial \bar{p}}{\partial x_i} + \frac{\partial \tau_{ij}}{\partial x_j} - \rho_{nf} \beta_{nf} (\bar{T} - T_c) g_i \quad (2)$$

$$\rho_{nf} \frac{\partial \bar{T}}{\partial t} + \rho_{nf} \bar{u}_i \frac{\partial \bar{T}}{\partial x_i} = -\frac{1}{c_{nf}} \frac{\partial q_i}{\partial x_i} \quad (3)$$

where,

$$\tau_{ij} = \mu_{nf} \left(\frac{\partial \bar{u}_i}{\partial x_j} + \frac{\partial \bar{u}_j}{\partial x_i} \right) - \rho_{nf} \overline{u'_i u'_j} \quad (4)$$

$$q_i = -k_{nf} \frac{\partial \bar{T}}{\partial x_i} + C_{nf} \rho_{nf} \overline{u'_i T'} \quad (5)$$

As a consequence of the time-averaging process of the Navier-Stokes equations, new terms are appeared in momentum and energy equations. They are the Reynolds stress tensor $(\rho_{nf} \overline{u'_i u'_j})$ and turbulent heat flux $(\rho_{nf} \overline{u'_i T'})$. Using eddy-viscosity models, these terms are modeled by analogy with the Stokes viscosity law and the Fourier heat conduction through the eddy viscosity (μ_t);

$$\rho_{nf} \overline{u'_i u'_j} = -\mu_t \left(\frac{\partial \bar{u}_i}{\partial x_j} + \frac{\partial \bar{u}_j}{\partial x_i} \right) \quad (6)$$

$$\rho_{nf} \overline{u'_i T'} = -\frac{\mu_t}{\sigma_T} \frac{\partial \bar{T}}{\partial x_i} \quad (7)$$

where μ_t and σ_t are the turbulent viscosity and the turbulent Prandtl number respectively.

2.1 Turbulence Model

The Low-Reynolds number (LRN) $k-\omega$ turbulence model of Wilcox [16] is used in this study because it has a good balance between accuracy, generality and computational cost. The turbulent kinetic energy (k) and the specific turbulent kinetic energy dissipation (ω) are given from their transport equations and the resulting $k-\omega$ equations, after taking Low-Reynolds number effects into account, can be written as;

$$\frac{\partial k}{\partial t} + \rho_{nf} \frac{\partial (\bar{u}_i k)}{\partial x_i} = \frac{\partial}{\partial x_i} \left[\left(\mu_{nf} + \frac{\mu_t}{\sigma_k} \right) \frac{\partial k}{\partial x_i} \right] + P_k + G_k - c_k f_k k \omega \quad (8)$$

$$\frac{\partial \omega}{\partial t} + \rho_{nf} \frac{\partial (\bar{u}_i \omega)}{\partial x_i} = \frac{\partial}{\partial x_i} \left[\left(\mu_{nf} + \frac{\mu_t}{\sigma_\omega} \right) \frac{\partial \omega}{\partial x_i} \right] + c_1 f_1 P_k + c_3 \frac{\omega}{k} G_k - c_2 \omega^2 \quad (9)$$

The eddy viscosity is obtained by:

$$\mu_t = c_\mu f_\mu \frac{\rho_{nf} k}{\omega} \quad (10)$$

The shear production and destruction of turbulent kinetic energy are respectively;

$$P_k = -\rho_{nf} \overline{u'_i u'_j} \frac{\partial \bar{u}_i}{\partial x_j} \quad \text{and}$$

$$G_k = -\beta_{nf} \rho_{nf} \overline{u'_i T'} g_i$$

Damping functions and constants of the LRN $k-\omega$ turbulence model are given below [16];

$$f_\mu = \frac{0.025 + R_t/6}{1 + R_t/6},$$

$$f_1 = \frac{0.1 + R_t/2.7}{(1 + R_t/2.7)} f_\mu \quad \text{and}$$

$$f_k = \frac{0.278 + (R_t/8)^4}{1 + (R_t/8)^4}$$

$$c_\mu=1, c_k=0.09, c_l=0.56, c_2=0.075, \sigma_k=2, \sigma_\omega=2$$

for c_3 is calculated as: [17],

$$c_3 = \tanh |\bar{v}/\bar{u}|$$

where R_t is the turbulence Reynolds number and it is calculated as:

$$R_t = \frac{\rho_{nf} k}{\omega \mu_{nf}}$$

2.2 Thermophysical Properties of Nanofluid

The effective properties of the nanofluid are defined as follows:

For the effective thermal conductivity and dynamic viscosity, K_{nf} and μ_{nf} , respectively, are calculated through the following empirical correlations obtained by Corcione [14] on the basis of a wide variety of experimental data available in the literature:

$$\frac{k_{nf}}{k_f} = 1 + 4.4 Re_p^{0.4} Pr_f^{0.66} \left(\frac{T}{T_{fr}} \right)^{10} \left(\frac{k_s}{k_f} \right)^{10} \phi^{0.66} \quad (11)$$

$$\frac{\mu_{nf}}{\mu_f} = \frac{1}{1 - 34.87 (d_p/d_f)^{-0.3} \phi^{1.03}} \quad (12)$$

These correlations include the effects of types of the base fluid and nanoparticles, diameter of nanoparticles, and temperature, and are very useful for numerical and analytical analysis of nanofluids heat transfer, Abouali and Ahmadi[15].

In equation (11), T is the nanofluid temperature, T_{fr} is the freezing point of the base liquid, and Re_p is the nanofluid particle Reynolds number defined as,

$$Re_p = \frac{\rho_f u_B d_p}{\mu_f} \quad (13)$$

where u_B is the nanoparticle Brownian velocity which can be obtained as the ratio of d_p and the diffusion time τ_D for particle displacement by a distance equal to d_p . This time scale can be approximated as $\tau_D = d_p^2/6D$, where $D = k_b T/3\pi\mu_f d_p$ represents the diffusion coefficient.

Substituting the τ_D and D in equation (13),

Re_p is given as, Corcione [14]:

$$Re_p = \frac{2\rho_f k_b T}{\pi\mu_f^2 d_p} \quad (14)$$

where $k_b = 1.38 \times 10^{-23}$ J/K is the Boltzmann's constant. d_f is the equivalent diameter of a base fluid molecule, given by:

$$d_f = \left(\frac{6M}{N\pi\rho_{f0}} \right)^{1/3} \quad (15)$$

Here M is the molecular weight of the base fluid, N is the Avogadro number, and ρ_{f0} is the density of the base fluid calculated at temperature $T_0=293$ K.

The other effective physical properties of the nanofluid are calculated according to the mixing theory, as typically done in the majority of the studies mentioned above.

The effective mass density of the nanofluid, ρ_{nf} , is given by:

$$\rho_{nf} = (1 - \phi)\rho_f + \phi\rho_s \quad (16)$$

The heat capacity per unit volume of the nanofluid, $(\rho c_p)_{nf}$, is

$$(\rho c_p)_{nf} = (1 - \phi)(\rho c_p)_f + \phi(\rho c_p)_s \quad (17)$$

Accordingly, the effective specific heat at constant pressure of the nanofluid, $(c_p)_{nf}$, is calculated as:

$$(c_p)_{nf} = \frac{(1 - \phi)(\rho c_p)_f + \phi(\rho c_p)_s}{(1 - \phi)\rho_f + \phi\rho_s} \quad (18)$$

The effective coefficient of thermal expansion of the nanofluid, β_{nf} , is defined by

$$(\rho\beta)_{nf} = -\frac{d\rho_{nf}}{dT} \quad (19)$$

Differentiate and substitute eq. (16) into eq. (19), and replace the temperature derivatives of ρ_f and ρ_s by the products $(\rho\beta)_f$ and $(\rho\beta)_s$ for the base fluid and the nanoparticles, respectively, yields:

$$(\rho\beta)_{nf} = (1 - \phi)(\rho\beta)_f + \phi(\rho\beta)_s \quad (20)$$

or

$$\beta_{nf} = \frac{(1 - \phi)(\rho\beta)_f + \phi(\rho\beta)_s}{(1 - \phi)\rho_f + \phi\rho_s} \quad (21)$$

2.3 Initial and Boundary Conditions

The fluid velocities at solid walls are equal to zero; temperatures are specified at the vertical walls as ($T=T_H$ for $x=0$ and $T=T_C$ for $x=L$, ($T_C < T_H$); adiabatic conditions are given as ($\partial T/\partial y=0$ for $y=0$ and $y=H$). For the LRN $k-\omega$ turbulence model, the boundary conditions are k is set to zero at walls and $\omega = 6\mu_n/\beta_0\rho_n y_p^2$ at the first node nearest the wall, as the value at the wall is theoretically infinity (being y_p the normal distance of the nearest node to the wall), **Wilcox [16]**. The fluid initial conditions are:

$$\bar{u} = 0, \quad \bar{v} = 0, \quad \bar{T} = T_{res} = T_C,$$

$$k = 0 \text{ and } \omega = 10^{-5} \text{ for } t = 0$$

The small initial value for Specific dissipation rate of kinetic energy is given for the convenience of turbulent viscosity evaluation.

2.4 Non-dimensional Formulation

Defining dimensionless variables as:

$$X = \frac{x}{H}, \quad Y = \frac{y}{H}, \quad t^* = \frac{tu_r}{H}, \quad U = \frac{\bar{u}}{u_r}, \quad V = \frac{\bar{v}}{u_r}$$

$$P = \frac{\bar{p}}{\rho_f u_r^2}, \quad \theta = \frac{\bar{T} - T_C}{T_H - T_C},$$

$$k^* = \frac{k}{u_r^2}, \quad \omega^* = \frac{\omega H}{u_r} \quad (23)$$

where u_r is defined as, **Incropera et al.[18]**:

$$u_r = \sqrt{g\beta_f\Delta T H}$$

and using these variables, the governing differential equations become:

$$\frac{\partial U}{\partial X} + \frac{\partial V}{\partial Y} = 0 \quad (24)$$

$$\rho_{nf}^* \frac{\partial U}{\partial t^*} + \rho_{nf}^* U \frac{\partial U}{\partial X} + \rho_{nf}^* V \frac{\partial U}{\partial Y} = -\frac{\partial P}{\partial X} +$$

$$\sqrt{\frac{Pr}{Ra}} \frac{\partial}{\partial X} \left[(\mu_{nf}^* + \mu_t^*) \left(\frac{\partial U}{\partial X} + \frac{\partial U}{\partial X} \right) \right] +$$

$$+ \sqrt{\frac{Pr}{Ra}} \frac{\partial}{\partial Y} \left[(\mu_{nf}^* + \mu_t^*) \left(\frac{\partial U}{\partial Y} + \frac{\partial V}{\partial X} \right) \right] \quad (25)$$

$$\rho_{nf}^* \frac{\partial V}{\partial t^*} + \rho_{nf}^* U \frac{\partial V}{\partial X} + \rho_{nf}^* V \frac{\partial V}{\partial Y} = -\frac{\partial P}{\partial Y} +$$

$$\sqrt{\frac{Pr}{Ra}} \frac{\partial}{\partial X} \left[(\mu_{nf}^* + \mu_t^*) \left(\frac{\partial V}{\partial X} + \frac{\partial U}{\partial Y} \right) \right] +$$

$$\sqrt{\frac{Pr}{Ra}} \frac{\partial}{\partial Y} \left[(\mu_{nf}^* + \mu_t^*) \left(\frac{\partial V}{\partial Y} + \frac{\partial V}{\partial Y} \right) \right] +$$

$$\rho_{nf}^* (\beta_{nf}/\beta_f) \theta \quad (26)$$

$$\rho_{nf}^* \frac{\partial \theta}{\partial t^*} + \rho_{nf}^* U \frac{\partial \theta}{\partial X} + \rho_{nf}^* V \frac{\partial \theta}{\partial Y} =$$

$$= \frac{1}{\sqrt{RaPr}} \frac{\partial}{\partial X} \left[\left(\mu_{nf}^* + \frac{\mu_t^* Pr_n}{\sigma_T} \right) \frac{\partial \theta}{\partial X} \right] +$$

$$\frac{1}{\sqrt{RaPr}} \frac{\partial}{\partial Y} \left[\left(\mu_{nf}^* + \frac{\mu_t^* Pr_n}{\sigma_T} \right) \frac{\partial \theta}{\partial Y} \right] \quad (27)$$

$$\rho_{nf}^* \frac{\partial k^*}{\partial t^*} + \rho_{nf}^* U \frac{\partial k^*}{\partial X} + \rho_{nf}^* V \frac{\partial k^*}{\partial Y}$$

$$= \sqrt{\frac{Pr}{Ra}} \frac{\partial}{\partial X} \left[\left(\mu_{nf}^* + \frac{\mu_t^*}{\sigma_k} \right) \frac{\partial k^*}{\partial X} \right] + \sqrt{\frac{Pr}{Ra}} \frac{\partial}{\partial Y} \left[\left(\mu_{nf}^* + \frac{\mu_t^*}{\sigma_k} \right) \frac{\partial k^*}{\partial Y} \right] + P_k + G_k$$

$$- c_k f_k \rho_{nf}^* k^* \omega^* \quad (28)$$

$$\begin{aligned} &\rho_{nf}^* \frac{\partial \omega^*}{\partial t^*} + \rho_{nf}^* U \frac{\partial \omega^*}{\partial X} + \rho_{nf}^* V \frac{\partial \omega^*}{\partial Y} \\ &= \sqrt{\frac{Pr}{Ra}} \frac{\partial}{\partial X} \left[\left(\mu_{nf}^* + \frac{\mu_t^*}{\sigma_\omega} \right) \frac{\partial \omega^*}{\partial X} \right] + \sqrt{\frac{Pr}{Ra}} \frac{\partial}{\partial Y} \left[\left(\mu_{nf}^* + \frac{\mu_t^*}{\sigma_\omega} \right) \frac{\partial \omega^*}{\partial Y} \right] + c_{1f1} \frac{\omega^*}{k^*} P_k^* \\ &+ c_3 \frac{\omega^*}{k^*} G_k^* - c_2 \rho_{nf}^* \omega^{*2} \end{aligned} \quad (29)$$

where, Ra and Pr are the Rayleigh number and Prandtl number, respectively;

$$\begin{aligned} P_k^* &= \mu_t^* \sqrt{\frac{Pr}{Ra}} \left[2 \left(\frac{\partial U}{\partial X} \right)^2 + 2 \left(\frac{\partial V}{\partial Y} \right)^2 + \left(\frac{\partial V}{\partial X} + \frac{\partial U}{\partial Y} \right)^2 \right] \\ G_k^* &= - \sqrt{\frac{Pr}{Ra}} \left(\frac{\mu_t^*}{\sigma_T} \right) \left(\frac{\beta_{nf}}{\beta_f} \right) \frac{\partial \theta}{\partial Y} \end{aligned} \quad (31)$$

and ,

$$\mu_t^* = \sqrt{\frac{Pr}{Ra}} c_{\mu f \mu} \frac{\rho_{nf}^* k^*}{\omega^*} \quad (32)$$

The dimensionless boundary conditions are written as;

$$\begin{aligned} \text{at } X = 0 & \quad \theta_{(0,Y)} = 1 \\ X = \frac{L}{H} & \quad \theta_{(L/H,Y)} = 0 \\ Y = 0 & \quad \left(\frac{\partial \theta}{\partial Y} \right)_{Y=0} = 0 \\ Y = 1 & \quad \left(\frac{\partial \theta}{\partial Y} \right)_{Y=1} = 0 \end{aligned}$$

For k and ω equations the boundary conditions will become; kinetic energy $k^* = 0$ at walls and normalized specific dissipation near the wall is:

$$\omega^* = \frac{6}{\beta_f} \sqrt{\frac{Pr}{Ra}} \frac{\mu_{nf}^*}{Y_f^2 \rho_{nf}^*}$$

3. Numerical procedure

The set of governing differential equations (Eqs. 24 to 29) which could be extracted in general form ,eq. (33), have been solved using finite-volume techniques.

$$\frac{\partial}{\partial t} (\rho \varphi) + \frac{\partial}{\partial x_j} (\rho u_j \varphi) = \frac{\partial}{\partial x_j} \left(\Gamma \frac{\partial \varphi}{\partial x_j} \right) + S_\varphi \quad (33)$$

The flow field is discretized into cells forming a staggered grid arrangement, **Fig.2**, and the general equation eq.(33) was converted into an algebraic equation with the following form:

$$a_p \varphi_p = \sum_{nb} a_{nb} \varphi_{nb} + a_o^o \varphi_o^o + S_u \quad (34)$$

where ‘nb’ and ‘o’ denote the coefficient for the neighbor grids and the old time step value, respectively.

Fully implicit time integration has been applied and a pressure based method of Semi-Implicit Method for Pressure-Linked Equations (SIMPLE) family is used to solve the velocity-pressure field coupling. Central

differences are employed to evaluate the diffusion terms. The convective terms are discretized by means of hybrid scheme. The source terms for k and ω equations have been linearized in the usual form to adding unconditional positive values to avoid the numerical instabilities.

Starting from specified initial values of the independent variables, i.e., specified initial temperature and velocity fields (as well as k and ω). An iterative through a line-by-line (LBL) application of the Thomas algorithm is adopted. Under-relaxation is introduced by means pseudo-transient for allowing and/or improving the rate of convergence. In order to capture the high gradient near the walls, a non-uniform grid has been used in all the calculations, with the grid clustered in the near-wall region to resolve the wall-damping effect. Within each uniform time step, the spatial solution is considered to be fully converged when the maximum absolute values of both the mass source and the percent changes of the independent variables at each grid-node from iteration to iteration are smaller than prescribed values (in this study equal to 10^{-4}). Then, the converged solution is used as the initial condition for the following time step. The method employed to solve the time differential terms is an unconditionally stable fully implicit scheme.

The Nusselt number, Nu , is expected to depend on a number of factors such as thermal conductivity, heat capacitance, viscosity, flow structure of nanofluids, volume fraction, dimensions, and fractal distributions of nanoparticles. The local Nusselt number can be expressed as:

$$Nu = - \frac{k_{nf}}{k_f} \frac{\partial \theta}{\partial X} \quad (33)$$

the average Nusselt number along the left wall (hot side) is given as:

$$\overline{Nu} = \int_0^1 Nu dY \quad (34)$$

The temperature gradients at both bottom and top walls are evaluated by assuming a second order temperature profile among each wall-node and the next two interior nodes. The integral is evaluated by the trapezoid rule.

4. Validation of the Numerical Code

In order to validate the present numerical code, the problem of turbulent natural convection of air in a differentially heated tall enclosure with an aspect ratio of 30 has been solved for Rayleigh number (based on enclosure height) equal to 2.43×10^{10} . The present results of vertical velocity component at enclosure mid line ($Y=0.5$) were compared to results of **Albets-Chico et al. [20]** for LRN $k-\omega$, and the experimental results of **Dafa'alla and Betts [21]** as shown in **Fig. 3**. A qualitative agreement is shown in this figure and a good validation is obtained as indicated in **Table 1** with maximum deviation of (6.5% and 4.4%). Further, a mesh testing procedure was conducted to guarantee a grid independent solution. Four different mesh combinations were explored for the case of $Ra=2.43 \times 10^{10}$, $Pr=0.7$. The present code was tested for grid independence by

calculating the average Nusselt number on the hot wall as shown in **Fig. 4** and **Table 2**. The results confirmed that the present numerical solution is a grid independent solution and grid size of 60×180 is used in this study.

5. Results and discussions

The turbulent natural convection heat transfer of water-based nanofluids in a differentially heated tall enclosure has been investigated numerically in this study. The right wall temperature of the enclosure is fixed at reference temperature 20 C° whereas the hot wall temperature is set to 40 C° . The computational results were obtained for Rayleigh numbers (based on enclosure height) range (10^{10} to 10^{12}) within three different aspect ratios (30, 40 and 50). The Prandtl number of the base fluid (water) is 7.1, and the nanoparticles volume fraction ϕ range was from 0% to 8%. Two types of nanoparticles, Al_2O_3 and Cu, are considered and the diameter of these suspended nanoparticles in the range 25-100 nm. The corresponding thermo-physical properties of the fluid and solid phases are given in **Table 3**. **Fig. 5** shows the effect of addition of nanoparticles on the thickness of the thermal boundary layer adjacent to the hot wall. Increasing the volume fraction ϕ causes the fluid to become more viscous and reduce the motion intensity of the nanofluid in the enclosure. This can be reflected by the expansion of the streamlines near the center of the enclosure. Slowing the flow motion tends to increase the thermal boundary layer thickness which responsible of reduction in temperature gradients at the hot surface. It must be noted that, since the effective thermal conductivity k_{nf} increase, the decrease of local temperature gradients at hot wall (also at cold wall) does not necessarily imply a degradation of the local heat transfer. To show that **Fig. 6** presented the distribution of the effective local Nusselt number along the hot wall Nu_h , and the distributions of local heat transfer coefficient $h_h = (Nu_h k)/H$, are presented in **Fig. 7** for the same values of ϕ , dp, ΔT and Ra previously used in **Fig. 5**. It may be seen that, fixed dp, ΔT and Ra , the amount of heat exchanged at $\phi=0.04$ is higher than transferred across the pure base fluid. Vice versa, at $\phi=0.08$ the heat transfer rate is lower, which means that the diminution of the temperature gradients at the sidewalls prevails on the increase of the effective thermal conductivity.

Fig. 8a presents that the vertical velocity increases close to the heated side of the enclosure and decreases close the cooled side due to the thermal buoyancy effects. Also, the magnitude of the vertical velocity decreases as the volume fraction increases since the fluid becomes more viscous as mentioned previously. A major effect of nanoparticles size on the vertical velocity component is reported in **Fig. 8b**.

Fig. 8c illustrates that nanofluid of lighter nanoparticle material have a higher vertical velocity as indicated for Cu-water and Al_2O_3 -water. The temperature distribution is found nonlinear and symmetric for all values of volume fraction as shown in **Fig. 8d**. However, as ϕ increases, the gradient of temperature decreases close to enclosure walls, i.e. it's shifted toward the center of the enclosure, due to higher thermal conductivity of the nanofluid. **Fig. 8e** shows a minor effect of nanoparticle size on the temperature variation. The temperature gradients of Cu-water nanofluid decreases more than of Al_2O_3 -water nanofluid for $\phi = 0.01$,

as presented in **Fig. 8f**. This behavior can be attributed to the increasing of the effective thermal conductivity according to eq. (11).

The evaluation of the heat transfer performance consequent to the addition of nanoparticles into the base fluid is expressed by the heat transfer enhancement, E, defined as [14];

$$E = \frac{Nu(\phi)}{Nu(\phi=0)} \times \frac{k_{nf}}{k_f} - 1 \quad (35)$$

Figures 9 to 12 display the effects of the nanoparticle size, the type of nanoparticles materials, enclosure aspect ratios and Rayleigh number on heat transfer enhancement E in the enclosure. It is apparent from the results that the heat transfer enhancement increases up to a point, which is due to the increase in effective thermal conductivity k_{nf} . **Corcione [11]** defined the value of ϕ which leads to maximize heat transfer enhancement E as the optimal particle loading and denoted as ϕ_{opt} . Increasing the volume fraction above ϕ_{opt} leads to decrease the heat transfer enhancement E which may be attributed to the excessive growth of the effective viscosity. **Fig. 9** shows that both the heat transfer enhancement E and ϕ_{opt} increases as nanoparticles size (dp) decreases due to increases the value of Re_p as in eq. (14) and this leads to increase the effective thermal conductivity. **Fig. 10** shows that the material that has a higher thermal conductivity gave a higher enhancement. Additionally, as expected, heat transfer enhancement E increases as Ra increased as shown in **Fig. 11** due to increase the buoyancy strength at higher values of Ra.

Fig. 12 displays the effect of the enclosure aspect ratio on the distributions of heat transfer enhancement E. The optimal particle loading ϕ_{opt} decreases with increasing aspect ratio H/L. As the enclosure width reduced with increasing the enclosure aspect ratio, the flow resistance decreasing and the growth of effective viscosity become excessive in comparison with growth of the effective thermal conductivity at higher values of ϕ .

6. Conclusions

Numerical simulations of turbulent natural convection of nanofluids inside a tall enclosure differentially heated at sides have been studied in the present study. On the basis of the presented results, the following conclusions may be extracted:

1. Heat transfer enhancement due to the presence of nanoparticles in the base fluid is found to increase with increasing nanoparticle volume fraction to a specify point called optimal volume loading, at which the maximum convective heat transfer is obtained, then it decreased with further increase of volume fraction.
2. Decreasing the diameter of the nanoparticles increases the heat transfer enhancement at optimum particle loading ϕ_{opt} .
3. The material of nanoparticles suspended in nanofluids has a pronounced effect on the enhancement heat transfer.
4. The optimal volume loading increases slightly as the Rayleigh number increase.

7. References

1. S.M. Fotukian, M. Nasr Esfahany, Experimental investigation of turbulent convective heat transfer of dilute γ -Al₂O₃/water nanofluid inside a circular tube, *International Journal of Heat and Fluid Flow* 31 (2010) 606–612.
2. M. Rostamani, S.F. Hosseinizadeh, M. Gorji, J.M. Khodadadi, Numerical study of turbulent forced convection flow of nanofluids in a long horizontal duct considering variable properties, *International Communications in Heat and Mass Transfer* 37 (2010) 1426–1431.
3. S. Özeriç, A.G. Yazıcıoğlu, S. Kakaç, Numerical analysis of laminar forced convection with temperature-dependent thermal conductivity of nanofluids and thermal dispersion, *International Journal of Thermal Sciences*, Volume 62, December 2012, Pages 138–14.
4. K. Khanafer, K. Vafai, M. Lightstone, Buoyancy-driven heat transfer enhancement in a two-dimensional enclosure utilizing nanofluids, *Int. J. Heat Mass Transfer* 46 (2003) 3639–3653.
5. R.Y. Jou, S.C. Tzeng, Numerical research of nature convective heat transfer enhancement filled with nanofluids in rectangular enclosures, *Int. Commun. Heat Mass Transfer* 33 (2006) 727–736.
6. H.F. Oztop, E. Abu-Nada, Numerical study of natural convection in partially heated rectangular enclosures filled with nanofluids, *Int. J. Heat Fluid Flow* 29 (2008) 1326–1336.
7. Elif Buyuk Ogut, Natural convection of water-based nanofluids in an inclined enclosure with a heat source, *International Journal of Thermal Sciences* 48 (2009) 2063–2073.
8. Kuang C. Lin, Angela Violi, Natural convection heat transfer of nanofluids in a vertical cavity: Effects of non-uniform particle diameter and temperature on thermal conductivity, *International Journal of Heat and Fluid Flow* 31 (2010) 236–245.
9. N. Putra, W. Roetzel, S.K. Das, Natural convection of nano-fluids, *Heat and Mass Transfer* 39 (8–9) (2003) 775–784.
10. D. Wen, Y. Ding, Formulation of nanofluids for natural convective heat transfer applications, *International Journal of Heat and Fluid Flow* 26 (6) (2005) 855–864.
11. A.G.A. Nnanna, Experimental model of temperature-driven nanofluid. *J. Heat Transfer* 129 (2007) 697-704.
12. E. Abu-Nada, F. Dinkelacker, A. Alatabi, B. Manickam, and S. Jollet, Heat Transfer Enhancement in a Differentially Heated Enclosure Using Nanofluids-Turbulent Regime, Porous media and its applications in science, engineering, and industry: 3rd International Conference. AIP Conference Proceedings, Volume 1254, (2010) 223-227.
13. Rui Ni, Sheng-Qi Zhou, and Ke-Qing Xia, An experimental investigation of turbulent thermal convection in water-based alumina nanofluid, *Physics of Fluids* 23, (2011) 022005.
14. Massimo Corcione, Heat transfer features of buoyancy-driven nanofluids inside rectangular enclosures differentially heated at the sidewalls, *International Journal of Thermal Sciences* 49 (2010) 1536-1546.
15. Omid Abouali, Goodarz Ahmadi, Computer simulations of natural convection of single phase nanofluids in simple enclosures: A critical review, *Applied Thermal Engineering* 36 (2012) 1-13.
16. D.C. Wilcox, Simulation of Transition with a Two-Equation Turbulence Model, *AIAA J.*32, (1994) 247-255.
17. R.A.W.M. Henkes, F.F. Van Der Vlugt, C.J. Hoogendoorn, Natural Convection Flow in a Square Cavity Calculated with Low-Reynolds-Number Turbulence Models, *Int. J. Heat Mass Transfer*, Vol.34,No.2 ,(1991) 377-388.
18. F.P. Incropera, D.P. DeWitt, T.L. Bergman, A.S. Lavine, *Fundamentals of Heat and Mass Transfer*, 6th ed., Joun Wily & Sons, New York (2007).
19. S.V. Patankar, *Numerical Heat Transfer and Fluid Flow*, Hemisphere, Washington, DC (1980).
20. X. Albet-Chico, A.Oliva, C.D Perez-Segarra, Numerical Experiments in Turbulent Natural Convection Using Two-Equation Eddy-Viscosity Models, *J. Heat Transfer*, Vol.130 (2008) ,072501-11.
21. A.A. Dafa'Alla and P.L. Betts, Experimental Study of Turbulent Natural Convection in a Tall Air Cavity, *Experimental Heat Transfer*, 9: (1996) 165-194.

Nomenclature

AR	Aspect Ratio (H/L)	N	Avogadro number = $6.022 \times 10^{23} \text{ mol}^{-1}$
$c_{\mu}, c_1,$ c_2, c_3	Coefficients of turbulent model	Nu	Nusselt number
d_f	Equivalent diameter of a base fluid molecule	P_k	Production of kinetic energy due to shear stresses
dp	Diameter of the nanoparticle	Pr	Prandtl number
E	Heat transfer enhancement	P	Mean pressure
f_1, f_2, f_{μ}	Damping functions of turbulence model	Ra	Rayleigh number (based on height) ($Ra = g\beta\Delta TH^3 Pr/\nu^2$)
g_i	Gravitational acceleration	Rt	Turbulence Reynolds number
G_k	Production of kinetic energy due to buoyancy effects	T	Mean temperature
H	Height of enclosure	t	Time
i, j	Vector direction	\bar{u}	Mean velocity in x-direction
k	Turbulent kinetic energy	U	Dimensionless velocity ($u/\sqrt{g\beta\Delta TH}$)
k_b	Boltzmann's constant = $1.38066 \times 10^{-23} \text{ J/K}$	\bar{v}	Mean velocity in y-direction
k^*	Dimensionless turbulent kinetic energy	V	Dimensionless velocity ($v/\sqrt{g\beta\Delta TH}$)
L	Width of enclosure	x, y	Cartesian coordinates
M	Molecular weight of the base fluid	X, Y	Dimensionless coordinates
Greek Symbols			
β	Thermal expansion coefficient	ν	Kinematic viscosity ($\nu = \mu/\rho$)
ϕ	Nanoparticle volume fraction	ρ	Density
μ	Dynamic viscosity	$\sigma_k, \sigma_t,$ $, \sigma_{\omega}$	Prandtl numbers for turbulence kinetic energy, temperature and dissipation of turbulence energy, respectively
μ_t	Eddy or turbulent viscosity	τ	Dimensionless time
μ_t^*	Dimensionless eddy or turbulent viscosity ($\mu_t^* = \mu_t/\mu$)	ω	Specific dissipation rate of kinetic energy
		ω^*	Dimensionless specific dissipation rate of kinetic energy ($\omega^* = \omega H/\sqrt{g\beta\Delta TH}$)
Subscripts			
C	Cooled sidewall of the enclosure	H	Hot sidewall of the enclosure
f	Base fluid	opt	Optimal value
nf	Effective (nanofluid) property		

Table 1: Comparison of numerical results obtained with numerical and experimental (for air, AR=30 and Ra= 2.34×10^{10}).

	Nu	$V_{\max} (Y=0.5)$	$\mu_t^* \max$
Numerical [19]	133.67 (-10.2%)	-	21.83 (-28%)
Present study	142.39 (-4.4%)	0.09658 (0.95%)	22.68 (-25%)
Experimental[20]	149.0	0.09567	30.40

Table 2: Grid independence study.

Grid size	Nu_{avg}
40 × 200	142.070
40 × 180	142.072
60 × 200	142.180
60 × 180	142.390

Table 3: Thermophysical properties of base fluid and nanoparticles.

Property	Base fluid (water)	Cu	Al ₂ O ₃
ρ (kg/m ³)	997.1	8933	3970
c_p (J/kg K)	4179	385	765
k (W/mK)	0.613	400	40
$\alpha \times 10^7$ (m ² /s)	1.47	1163.1	131.7
β (K ⁻¹)	0.00021	0.000051	0.000024

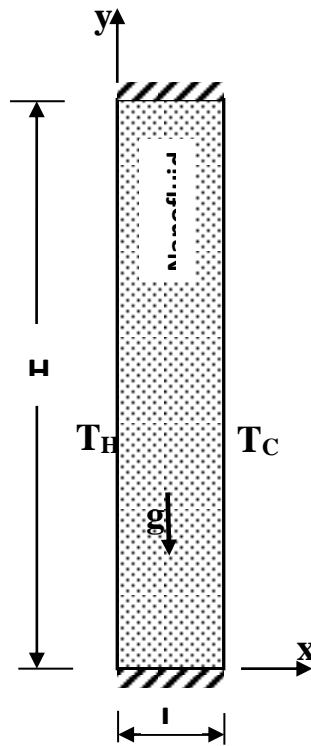


Fig.1 Geometry and coordinate system.

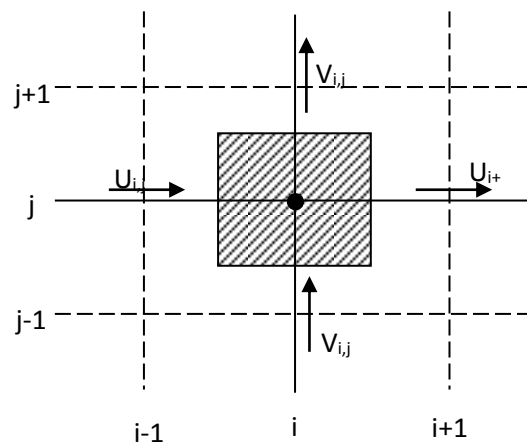


Fig. 2 A typical control volume showing the locations of the principle variables - Scalar variables at point (i,j) , $P_{i,j}$, $T_{i,j}$, $k_{i,j}$, $\omega_{i,j}$,..... - $U_{i,j}$ and $V_{i,j}$ at staggered grids.

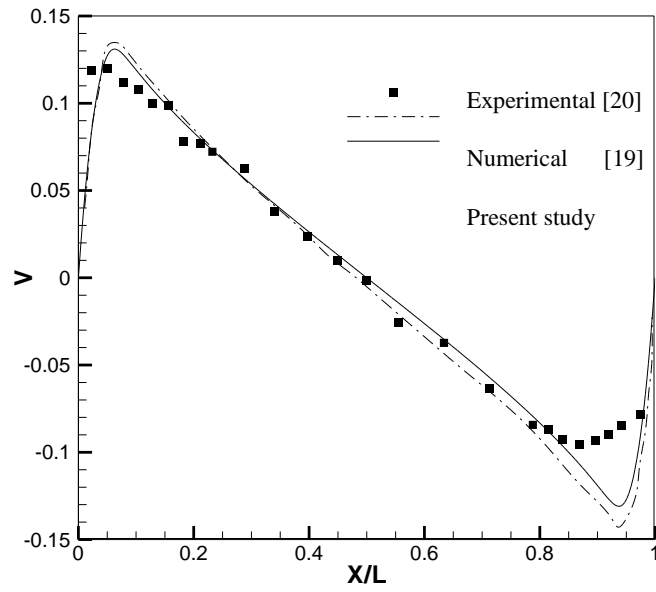


Fig. 3 Comparison of V-velocity profiles of air at Y=0.5 in the cavity of AR=30 and Ra=2.43×10¹⁰

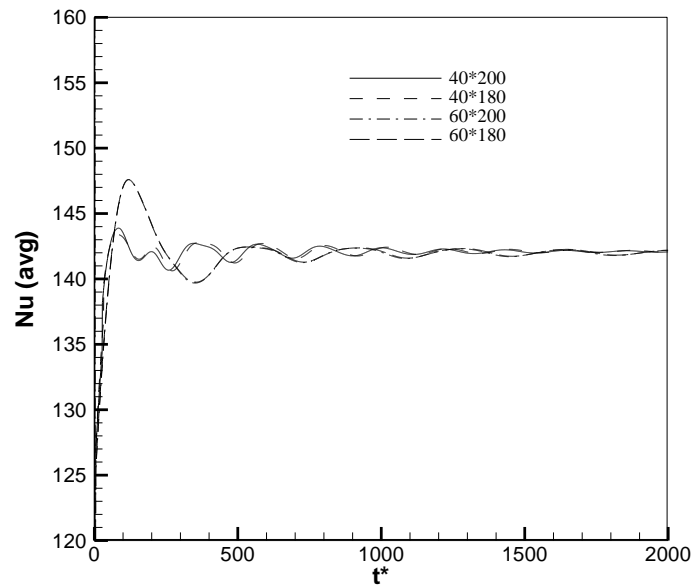


Fig. 4 Variation of average Nusselt no. for different grid size (AR=30 and Ra=2.43×10¹⁰)

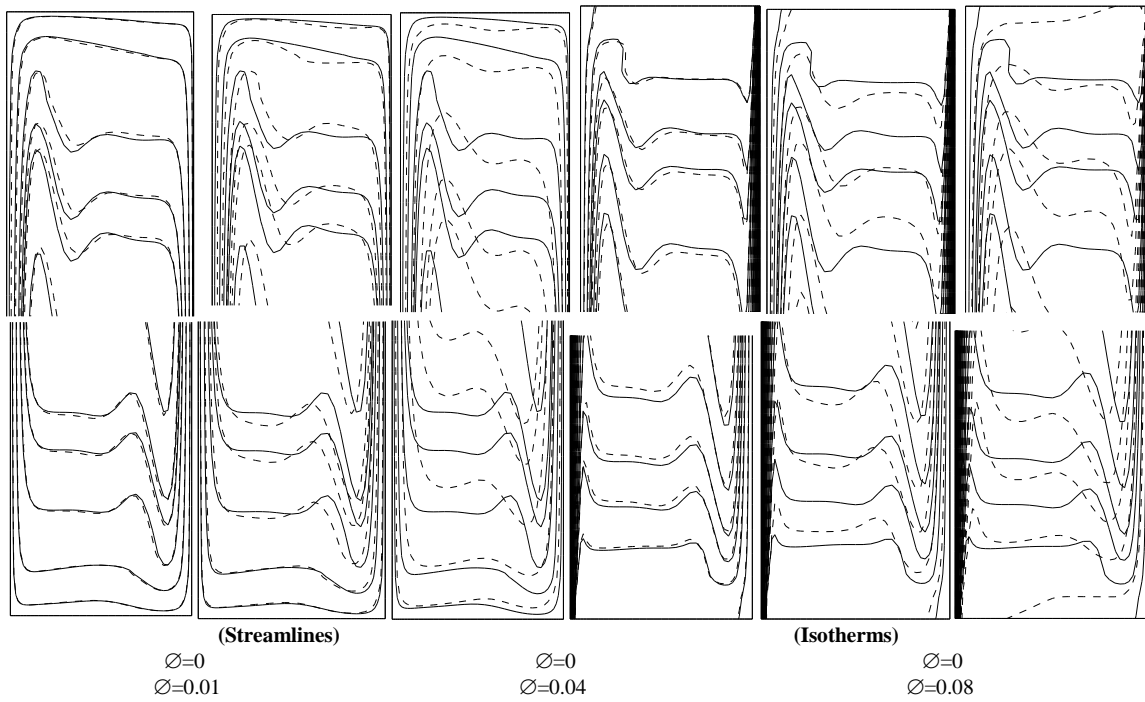


Fig. 5 Streamlines and isotherms of a Al_2O_3 -water nanofluid for $Ra=10^{12}$, $AR=40$, and $dp=25$ nm.

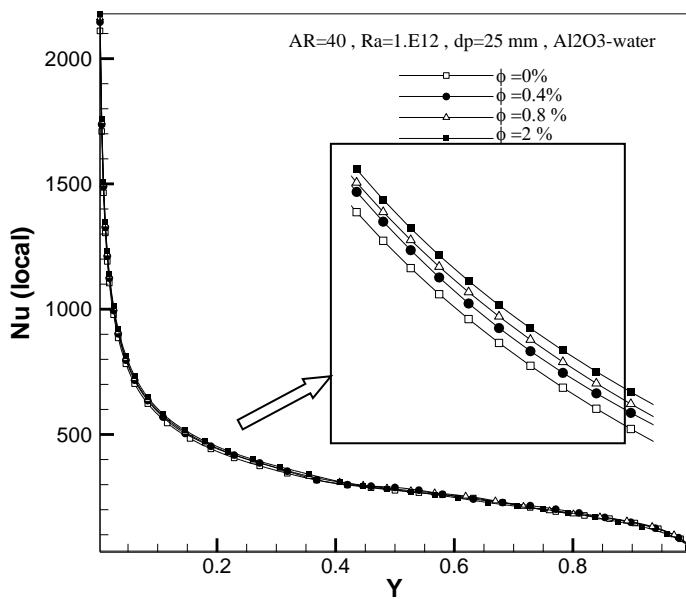


Fig. 6 Distributions of the local effective Nusselt number for different volume fraction.

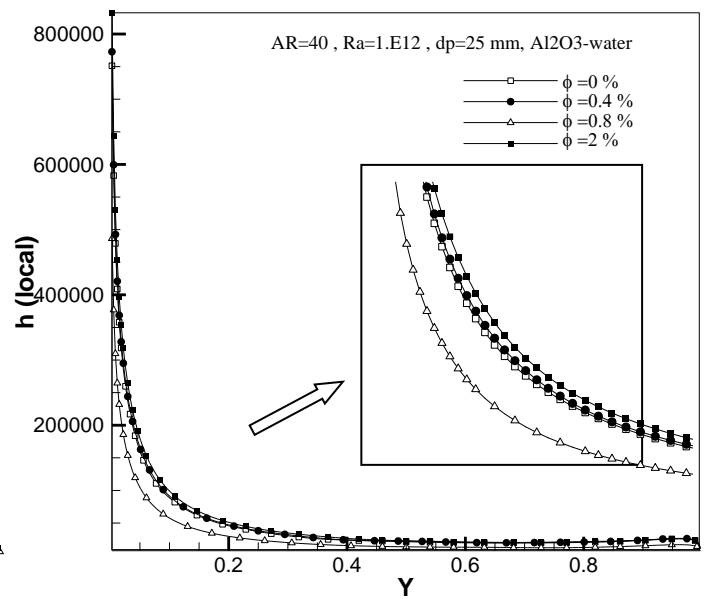


Fig. 7 Local heat transfer coefficient along hot wall for different volume fraction.

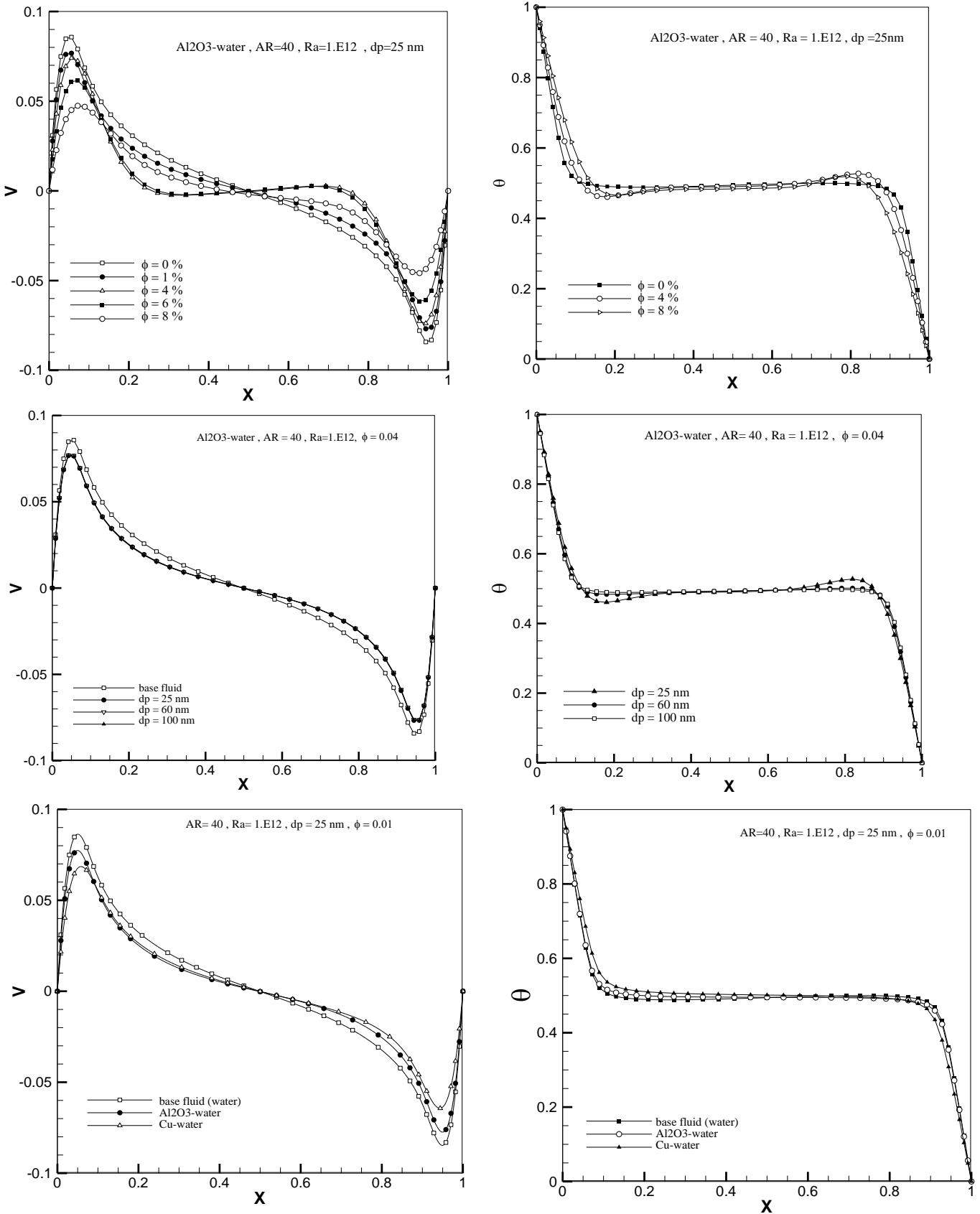


Fig. 8 Velocity and temperature distributions for water and nanofluid at $Y=0.5$.

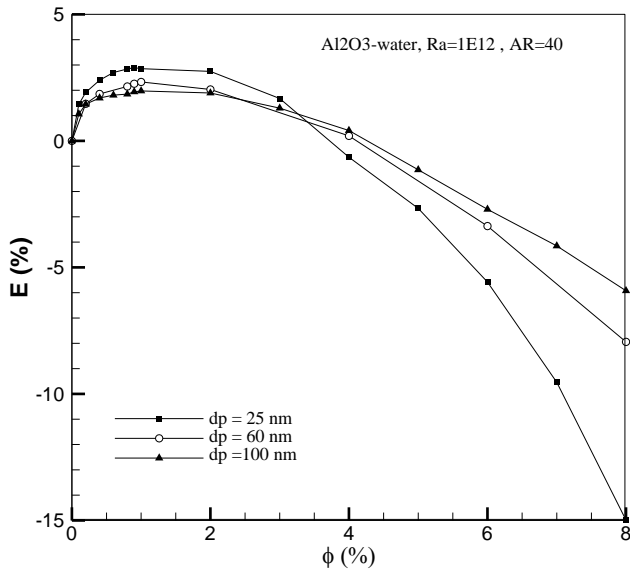


Fig. 9 Variation of E(%) with volume fraction for different dp

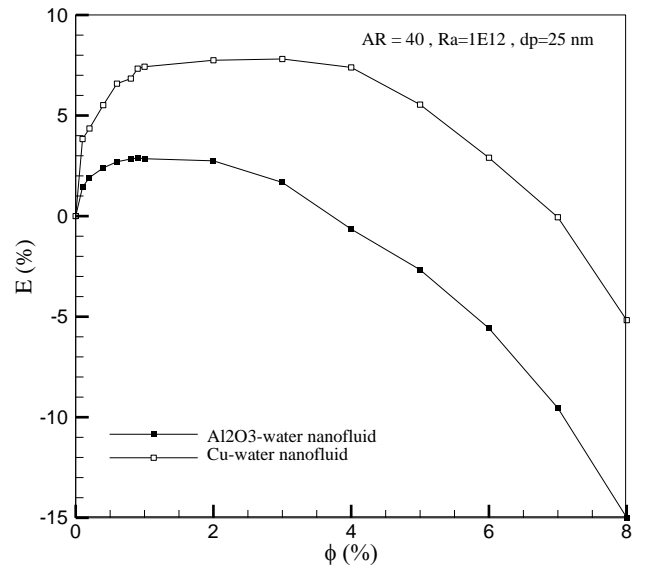


Fig. 10 Variation of E(%) with volume fraction for different types of nanoparticles

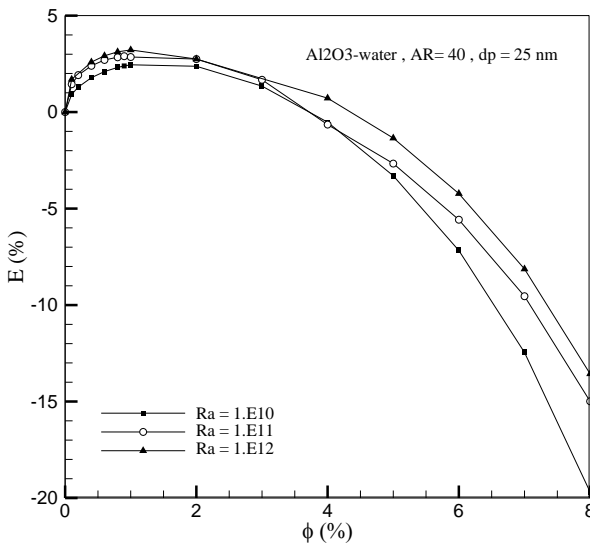


Fig. 11 Variation of E(%) with volume fraction for different Ra no.s

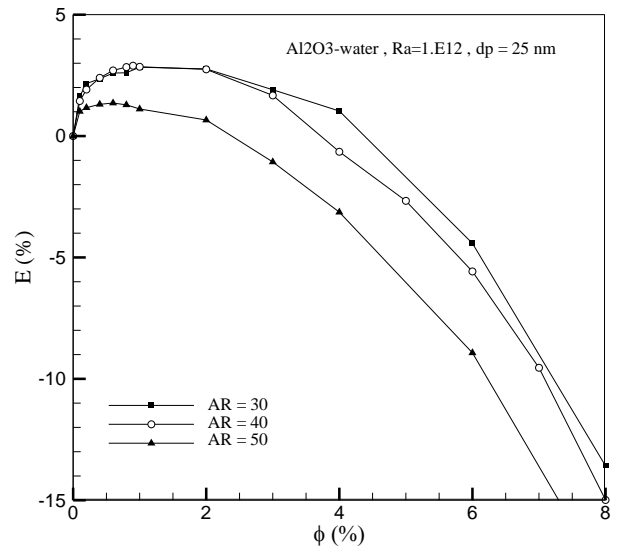


Fig. 12 Variation of E(%) with volume fraction for different AR